catalysts

MDPI

Article

Nitrogen-Rich Tetrazole–Amide-Functionalised Zn Metal–Organic Framework as Catalyst for Efficient Catalytic CO_2 Cycloaddition with Epoxides

Anup Paul [1,*], Ismayil M. Garazade [1,2], Anirban Karmakar [1], Rais Ahmad Khan [3], Maria Fátima C. Guedes da Silva [1,4], Ana V. M. Nunes [5] and Armando J. L. Pombeiro [1,*]

1 Centro de Química Estrutura, Institute of Molecular Sciences, Instituto Superior Técnico, Universidade de Lisboa, Av. Rovisco Pais, 1049-001 Lisboa, Portugal; ismayil.garazade@gmail.com (I.M.G.); anirbanchem@gmail.com (A.K.); fatima.guedes@tecnico.ulisboa.pt (M.F.C.G.d.S.)
2 Department of Chemistry, Baku State University, Z. Khalilov Str. 23, 1148 Baku, Azerbaijan
3 Department of Chemistry, King Saud University, Riyadh 11451, Saudi Arabia
4 Departamento de Engenharia Química, Instituto Superior Técnico, Universidade de Lisboa, Av. Rovisco Pais, 1049-001 Lisboa, Portugal
5 LAQV-REQUIMTE, Departamento de Química, Faculdade de Ciências e Tecnologia, Universidade Nova de Lisboa, 2829-516 Caparica, Portugal
* Correspondence: anuppaul@tecnico.ulisboa.pt (A.P.); pombeiro@tecnico.ulisboa.pt (A.J.L.P.)

Abstract: In this study, we report the design, synthesis, and catalytic application of the novel nitrogen-rich Zn(II) MOF $[Zn_2(\mu_3\text{-}1\kappa N,2\kappa N',3\kappa O\text{-}HL)_2(DMF)_2]_n \cdot nH_2O$ (HL^{2-} = 4-((4-(1H-tetrazol-5-yl)phenyl)carbamoyl)benzoate), denoted as **ZnMOF**, for the efficient conversion of carbon dioxide (CO_2) to cyclic carbonates via cycloaddition with epoxides. It was synthesised from a tetrazole appended amide-functionalised pro-ligand ($\mathbf{H_3L}$) and $Zn(NO_3)_2 \cdot 6H_2O$ under hydrothermal conditions. The synthesised material was characterised namely by elemental analysis, infrared spectroscopy, powder X-ray diffraction (PXRD), and single-crystal X-ray diffraction analyses. The catalytic potential of **ZnMOF** was investigated in the CO_2 cycloaddition reaction with various epoxides, with conversions ranging from 17% to 99%. The catalyst retained its activity across multiple reaction cycles, demonstrating its stability and reusability. The influence of co-catalysts on the reaction was explored, with tetrabutylammonium bromide (TBABr) emerging as the most effective one. A plausible reaction mechanism is proposed.

Keywords: tetrazole; amide functionalised; MOF; CO_2; epoxides

Citation: Paul, A.; Garazade, I.M.; Karmakar, A.; Khan, R.A.; Guedes da Silva, M.F.C.; Nunes, A.V.M.; Pombeiro, A.J.L. Nitrogen-Rich Tetrazole–Amide-Functionalised Zn Metal–Organic Framework as Catalyst for Efficient Catalytic CO_2 Cycloaddition with Epoxides. *Catalysts* **2024**, *14*, 6. https://doi.org/10.3390/catal14010006

Academic Editor: Min Kim

Received: 30 October 2023
Revised: 5 December 2023
Accepted: 15 December 2023
Published: 20 December 2023

1. Introduction

In recent years, the field of coordination chemistry has made significant strides in the wide range of applications offered by metal-organic frameworks (MOFs) and coordination polymers [1–4]. These materials have gained considerable attention in diverse fields, such as catalysis, gas storage, drug delivery and sensing, due to their tunable structures, porosity, and unique properties [1–12]. As a result, the design and synthesis of innovative ligands capable of forming well-defined coordination polymers have become a focal point of research [9,13,14]. However, achieving precise control over the design and synthesis of coordination frameworks with desired functionalities remains a formidable challenge, necessitating a deeper understanding of the factors that govern their formation. An effective approach involves the strategic design of organic ligands with suitable shape, functionality, flexibility, and symmetry, coupled with consideration of the coordination geometry of the metal ions and reaction conditions.

One prominent class of ligands widely utilised in MOF and coordination polymer construction consists of carboxylate-based ones [15]. These ligands, particularly benzene

dicarboxylates and benzene tricarboxylates, exhibit excellent coordination abilities, enabling the formation of robust frameworks with high porosity and adjustable properties. Their versatility lies in their capacity to coordinate with various metal ions, resulting in a broad spectrum of structures and functionalities [15]. Additionally, ligands featuring flexible dithioether and disulfoxide functionalities have been extensively explored for their ability to introduce structural adaptability and dynamic behaviour in coordination polymers [16,17]. These ligands offer conformational flexibility, facilitating the development of coordination polymers with responsive frameworks and tailored properties.

Recent advancements in ligand design have focused on incorporating multiple functionalities within a single ligand molecule, leading to the emergence of ditopic and multitopic ligands [18,19]. These ligands possess multiple binding sites, enabling the construction of complex coordination polymers with intricate topologies and tailored properties [18,19]. For instance, azole heterocycles and carboxylate groups, known for their exceptional coordination capabilities and diverse coordination modes, have shown interest in the synthesis of coordination polymers [18–20]. Ligands that combine carboxylate and N-heterocyclic groups have been successfully employed to create well-defined coordination polymers [18–20]. Among these ligand families, tetrazole stands out as a compelling building block due to its electron-donating capability via its four nitrogen atoms [10,20–23]. This unique attribute allows tetrazole to serve as either a multidentate ligand or a bridging building block in supramolecular assemblies. Nonetheless, despite extensive research on various ligands for coordination polymer synthesis, ligands based on tetrazole–benzoate building blocks have remained relatively underexplored [24–27]. These ditopic ligands hold significant potential as versatile building blocks for constructing coordination polymers with novel topologies and tailored properties, and the combination of tetrazole and benzoate moieties presents an exciting platform for the rational design and synthesis of functional coordination frameworks.

Our research endeavours have centred on the design and synthesis of amide-functionalised ligands for the construction of MOFs and coordination polymers [28–33]. The incorporation of amide groups serves to create open coordination sites within the frameworks, facilitating gas adsorption, storage, and wastewater treatment due to amide interactions, which enhance gas sorption capacity and selectivity [28–35]. Furthermore, our work has yielded several coordination polymers that exhibit excellent catalytic performance in cyanosilylation reactions of aldehydes, with potential applications in wastewater treatment, supercapacitors, and electrocatalysis for oxygen and hydrogen reactions [28–34]

In this manuscript, we explore a new ligand based on tetrazole–amide–benzoate motifs for the construction of MOFs. Specifically, we highlight the design, synthesis, and characterisation of a novel tetrazole–amide–benzoate-based ligand and its zinc(II) MOF. This MOF demonstrates promising catalytic performance in the CO_2 cycloaddition reaction with epoxides, yielding cyclic carbonates as the desired products.

2. Results and Discussion

2.1. Syntheses and Characterisation

The pro-ligand **H_3L** was synthesised through a multi-step process. Initially, 4-aminobenzonitrile was reacted with methyl 4-(chlorocarbonyl)benzoate and triethylamine in an anhydrous THF. Subsequently, the obtained product was treated with NaN_3 and NH_4Cl and subjected to hydrolysis, following an established procedure [28,29,36]. To synthesise the nitrogen-rich Zn(II) coordination polymer, a solution of **H_3L** in DMF was combined with an aqueous solution of $Zn(NO_3)_2{\cdot}6H_2O$ under hydrothermal conditions, as depicted in Scheme 1.

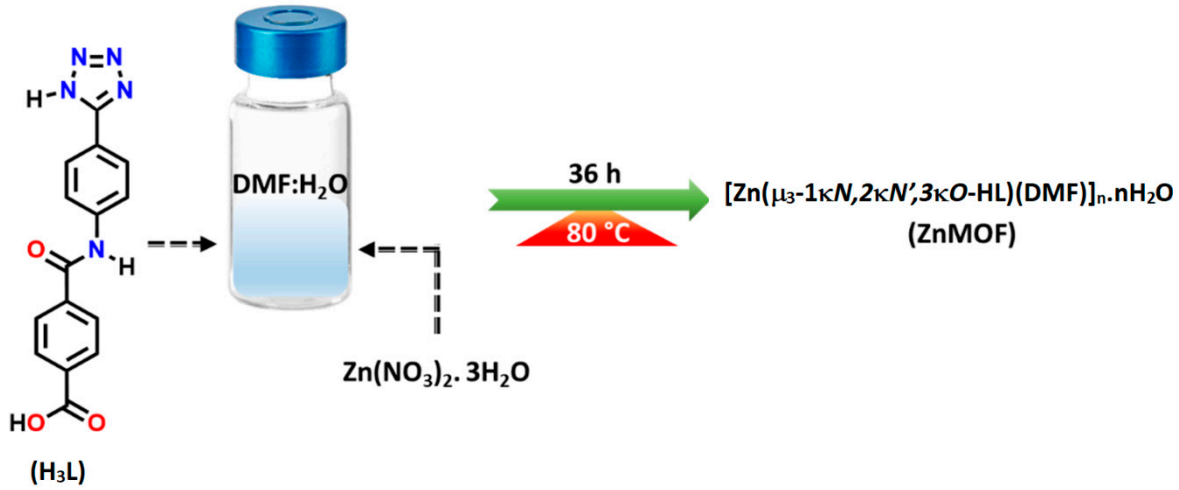

Scheme 1. Synthesis of **ZnMOF**.

The formation of the pro-ligand (**H_3L**) was confirmed through a wide range of analytical approaches encompassing elemental analysis, infrared spectroscopy, as well as ^{1}H and ^{13}C NMR spectroscopy. In the ^{1}H NMR spectrum, **H_3L** exhibits distinctive resonances attributed to the –COOH and –NH protons, at δ13.41 and 10.82, respectively (Figure S1). The protons associated with the phenyl ring resonate within the range of δ8.09–7.83. In the ^{13}C NMR spectrum, the signal corresponding to the –COOH group appears at δ167.1, accompanied by other resonances at their typical positions (Figure S2). On the other hand, validation of the formation of the nitrogen-rich Zn(II) coordination polymer was attained by utilising infrared spectroscopy, powder X-ray diffraction (PXRD) and single crystal X-ray diffraction analysis.

The infrared spectra of **H_3L** and **ZnMOF** are depicted in Figure S3. In the IR spectrum of **H_3L**, the presence of a peak at 1703 cm^{-1} is attributed to the asymmetric stretching vibration of the carbonyl group [ν_{asym}(COO)]. Notably, this vibration gradually diminishes, while a new vibration emerges at 1671 cm^{-1} in **ZnMOF**, signifying the coordination of the carboxylate group [28,29]. The revelation of the molecular structure was further elucidated through single-crystal X-ray diffraction analysis, as elaborated below.

Additionally, a thorough assessment of the congruity between the crystal structure and the synthesised bulk material was pursued through powder X-ray diffraction (PXRD) analysis. Through the comparison of experimental PXRD data with computationally simulated patterns, confirmation of alignment was achieved, further substantiating the coherence between the crystal structure and the synthesised bulk material, as depicted in Figure S4. During analysis, minor discrepancies in intensity were noted between the experimental and calculated patterns. These distinctions are presumably linked to factors like differing crystal orientations, potential interpenetration of faces, or potential inclusion of solvent guest molecules within the MOF structure's cavities [37,38].

2.2. Crystallographic Analysis of Zn-MOF

The X-ray diffraction analysis of the MOF, formulated as [Zn_2(μ_3-1κ*N*,2κ*N*′,3κ*O*-HL)$_2$(DMF)$_2$]$_n$·nH_2O (**ZnMOF**) (HL^{2-} = 4-[{4-(5H-tetrazol-5-yl)phenyl}carbamoyl]benzoate; DMF = dimethyl formamide), showed that it crystallises in a triclinic P-1 space group. The asymmetric unit has two symmetrically independent Zn(II) centres (Zn1 and Zn2), two 4-[{4-(5H-tetrazol-5-yl)phenyl}carbamoyl]benzoate (L) ligand, two coordinated DMF and one non-coordinated water molecule (Figure 1a). Every Zn(II) cation adopts a tetrahedral geometry (τ4 = 0.86–0.90) [39] constructed from a $N_{tetrazole}$ atom from two neighbouring L ligands and an $O_{carboxylate}$ atom from a third one, the remaining coordination position being occupied by a DMF molecule. The distances between the Zn cations and the uncoordinated $O_{carboxylate}$ atoms are quite different: 2.92(1) Å for Zn1···O2 and 2.67(1) Å for

Zn2···O5, the latter cation approaching a five-coordinate geometry by means of a chelating carboxylate group. The HL^{2-} ligand coordinates simultaneously with three different Zn(II) ions. The planarity of the two HL^{2-} ligands differ considerably with one of them being noticeably twisted relative to the other, as measured by the angles between the least-square planes of their phenyl groups: 12.49° in one ligand and 76.84° in the other.

The Zn-O bond length ranges from 1.906(9) to 1.975(8) Å, and the Zn-N ones from 1.995(10) to 2.015(10) Å. The O–Zn–O, N–Zn–O and N–Zn–N bond angles assume values of 116.4(4)°–123.0(4)°, 99.8(4)°–117.1(4)° and 113.1(4)°–116.0(4)°, respectively (Table S2). The intrapolymer Zn1···Zn2 distance is of 6.120(3) Å, higher than the interpolymer one, 5.667(3) Å, despite the same Zn1···Zn1 or Zn2···Zn2 distance of 7.9744(4) Å.

The tetrazole units of the HL^{2-} ligands connect the zinc ions forming a 1D zig-zag chain along the crystallographic *b* direction as shown in Figure 1b. These chains are joined by the 4-(phenylcarbamoyl)benzoate units to generate the 2D framework of **ZnMOF** having small rectangular channels (Figure 1c,d).

The NH groups of HL^{2-} and the water molecules are responsible for hydrogen bond interactions in **ZnMOF**. The former obey to $S_1^1(18)$ and to $R_1^1(18)$ patterns by acting as donor (intra- and inter-molecularly, respectively), to the O_{amide} atom. The latter generates $R_2^2(32)$ arrays resulting from combination of $D_1^1(2)$ motifs where the water molecule simultaneously donates to two non-coordinated $O_{carboxylate}$ atoms.

The non-coordinated $N_{tetrazole}$ atoms can act as acceptors of H_{methyl} atoms of DMF. Topological analysis of framework **ZnMOF** discloses that the Zn(II) atom and ligand L are 3-connected, thus it has a 3-connected uninodal net with topological type fes; Shubnikov plane net (4.8^2) (Figure 1e).

2.3. Thermogravimetric Analysis

To gain insights into the thermal stability of the framework **ZnMOF**, we conducted thermogravimetric analysis (TGA) under a dinitrogen atmosphere. This analysis was carried out over a temperature range spanning from 30 to 800 °C, utilising a controlled heating rate of 10 °C per minute.

The TGA result for **ZnMOF** is presented in Figure S5. The observed weight loss profile entails two distinct stages. Initially, a weight loss of 2.25% (calculated as 1.98%) occurs within the temperature range of approximately 50–105 °C, which can be attributed to the removal of one non-coordinated water molecule. Subsequently, a more substantial weight loss of 15.3% (calculated as 16%) transpires during the interval of 125–300 °C. This weight loss corresponds to the loss of two-coordinated DMF molecules. As the temperature surpasses 300 °C, the polymeric structure disintegrates, leading to the generation of ZnO.

2.4. BET Surface Area Analysis and Porosity Measurement Using Nitrogen Adsorption-Desorption Isotherm

In our investigation of the **ZnMOF**'s porosity, we employed N_2 sorption isotherms and applied the Brunauer–Emmett–Teller (BET) adsorption/desorption model (as depicted in Figure 2). The tests, conducted at 77 K, revealed type IV isotherms, consistent with IUPAC guidelines [40]. The BET surface area for the **ZnMOF** was determined to be relatively modest, measuring at 30.6 m^2/g.

Furthermore, we conducted a pore size distribution analysis using the NLDFT method, and the results are shown in Figure 2b. The observed peaks in this distribution plot signify a significant concentration of micropores falling within the approximate range of 1–2.5 nm.

2.5. Catalytic Studies

In this study, we explored the catalytic potential of our synthesised **ZnMOF** catalyst in facilitating the CO_2 cycloaddition reaction with epoxides to produce cyclic carbonates, as depicted in Scheme 2.

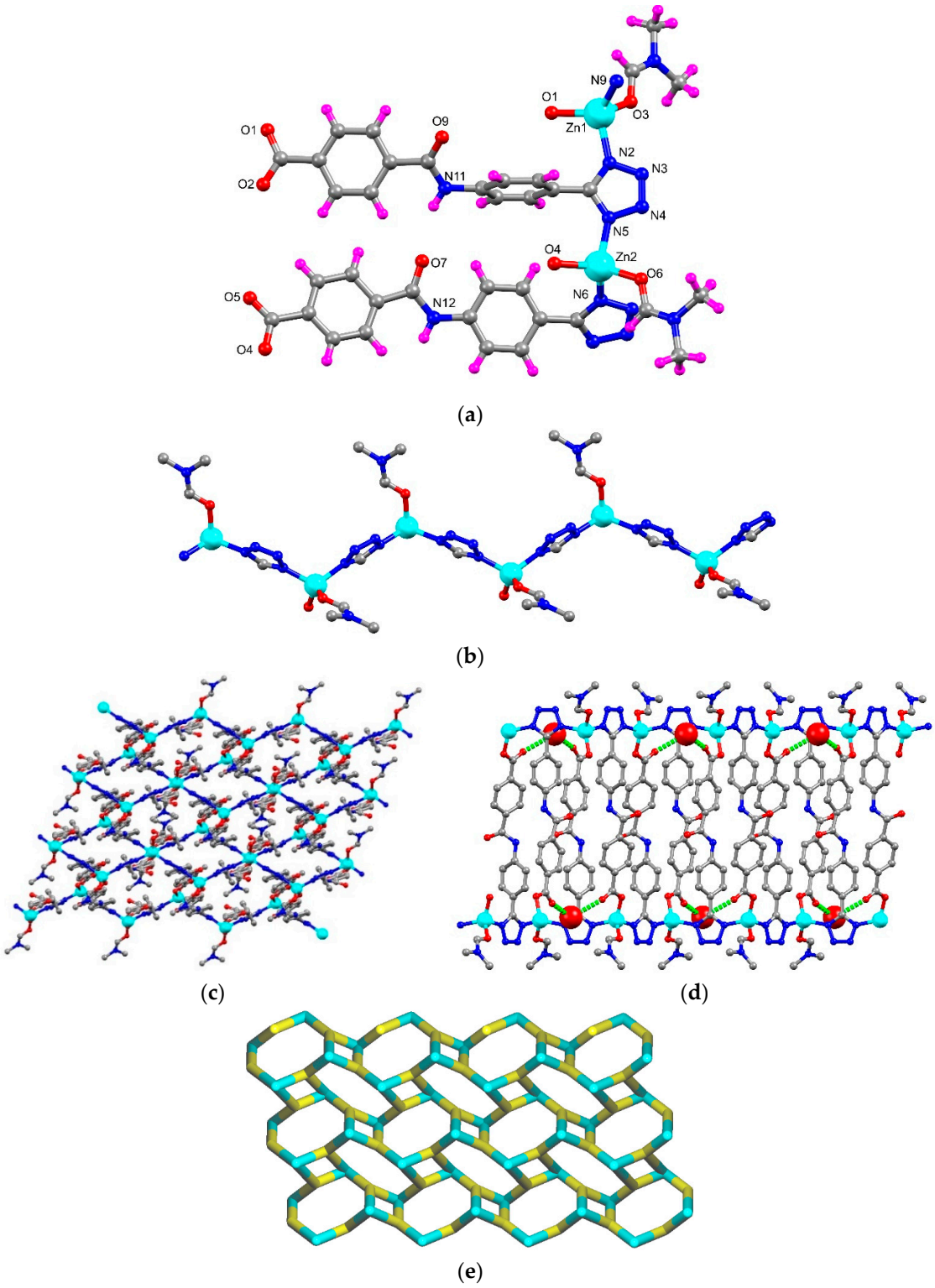

Figure 1. (**a**) Asymmetric unit of **ZnMOF** with partial atom labelling scheme; (**b**) 1D zig-zag structure constructed by tetrazole unit and Zn(II) atoms; (**c**) 2D network of **ZnMOF** presented in ball-stick; (**d**) hydrogen bonding interactions between **ZnMOF** and non-coordinated water molecules [water molecules are represented in space-filling models and H-bonding interactions are in green dotted lines; (**e**) node-and-linker-type representation of **ZnMOF** (the metal nodes are represented in cyan and the linker HL^{2-} in yellow colour).

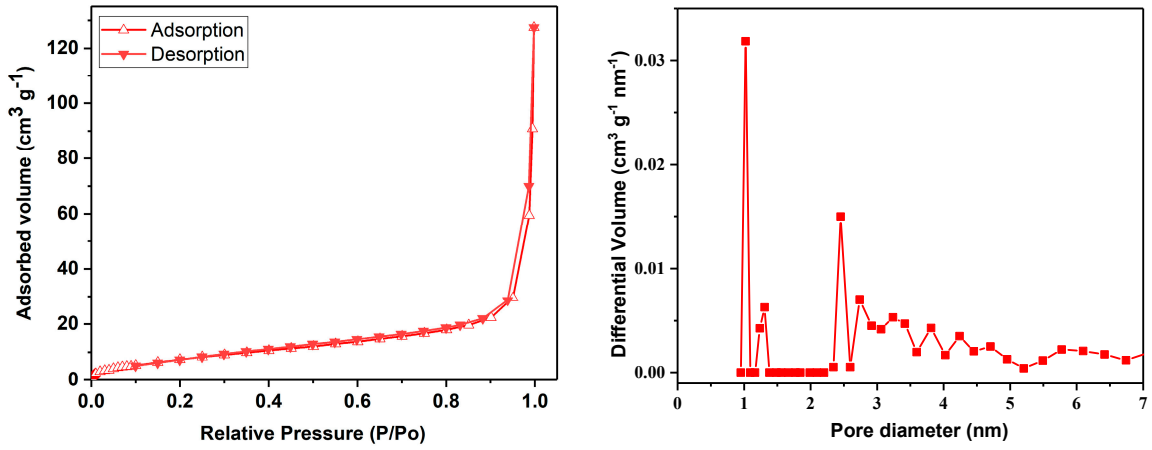

(**a**) (**b**)

Figure 2. N_2 adsorption isotherm at 77 K for the **ZnMOF** (**a**) and NLDFT PSD (pore size distribution) (**b**).

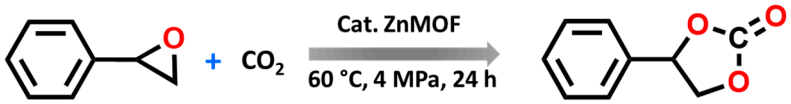

Scheme 2. Model reaction for carbonate formation using **ZnMOF** as the catalyst.

Preliminary catalytic tests were performed to assess the potential of **ZnMOF** as catalysts for the cycloaddition reaction between CO_2 and epoxides. We initiated our experiments by selecting styrene oxide as a model substrate and conducting the reaction in a stainless-steel cylindrical reactor using TBABr as a co-catalyst. The mixture was stirred at 60 °C for 24 h at a pressure of 4 MPa, and subsequent ^{1}H NMR spectroscopy allowed us to determine the substrate conversion (Table 1, Figure S7).

Initial experimentation converted a high ca. 90% of styrene oxide at 60 °C and 4 MPa CO_2 pressure using 0.20 mol% catalyst (entry 1, Table 1). We then systematically optimised the reaction conditions by varying reaction time, catalyst loading, and temperature.

Experiments were carried out at various time intervals, including 3, 8, 12, 18, 24, and 36 h (entries 2–7, Table 1, Figure 3a). Initial results at 3 h revealed a relatively modest conversion of ca. 25%. However, as the reaction time was extended to 8, 12, and 18 h, a notable increase in conversion was observed (entries 3–6, Table 1). The pinnacle of the reaction was reached after 24 h, resulting in the highest conversion (ca. 90%). Further extension of the reaction duration to 36 h led to only a marginal improvement in epoxide conversion, as depicted in entry 7, Table 1.

We also investigated the influence of catalyst loading (from 0.10 to 0.25 mol%) on the conversion of the reaction (entries 9–12, Table 1, Figure 3b). A catalyst loading of 0.20 mol% yields the highest conversion (entry 11, Table 1). Further deviations from this loading, specifically increasing to 0.25 mol% (entry 12, Table 1) or decreasing to 0.15 and 0.10 mol% (entries 9 and 10, Table 1), did not result in more favourable conversions.

Furthermore, we also tested our catalyst performance by varying the temperature. Conversions decreased below 60 °C, while no significant change was observed above 60 °C (Table 1, entries 13–15). We also examined the pressure effect within the 3–6 MPa range (entries 16–18, Table 1). The most favourable results were achieved when the pressure was set at 4 MPa (entry 17, Table 1), beyond which only a slight increase in the conversion was observed.

Table 1. Effect of co-catalyst, reaction time, amount of catalyst, temperature, and pressure on **ZnMOF** catalysed cycloaddition of CO_2 with styrene oxide.

Entry	Catalyst	Time (h)	Catalyst Amount (mol%)	CO_2 Pressure (MPa)	T (°C)	Conversion [a] (%)
1	**ZnMOF** [b]	24	0.20	4	60	89.6
2	**ZnMOF** [b]	3	0.20	4	60	24.5
3	**ZnMOF** [b]	8	0.20	4	60	46.8
4	**ZnMOF** [b]	12	0.20	4	60	73.8
5	**ZnMOF** [b]	18	0.20	4	60	80.9
6	**ZnMOF** [b]	24	0.20	4	60	89.6
7	**ZnMOF** [b]	36	0.20	4	60	90.0
8	**ZnMOF** [b]	24	0.00	4	60	14.9
9	**ZnMOF** [b]	24	0.10	4	60	45.7
10	**ZnMOF** [b]	24	0.15	4	60	74.5
11	**ZnMOF** [b]	24	0.20	4	60	89.6
12	**ZnMOF** [b]	24	0.25	4	60	89.7
13	**ZnMOF** [b]	24	0.20	4	40	79.2
14	**ZnMOF** [b]	24	0.20	4	60	89.6
15	**ZnMOF** [b]	24	0.20	4	80	90.0
16	**ZnMOF** [b]	24	0.20	3	60	82.2
17	**ZnMOF** [b]	24	0.20	4	60	89.6
18	**ZnMOF** [b]	24	0.20	6	60	90.3
19	$Zn(NO_3)_2{\cdot}6H_2O$ [b]	24	0.20	4	60	51.5
20	**H_3L** [b]	24	0.20	4	60	15.6
21	**ZnMOF** [c]	24	0.20	4	60	38.4
22	**ZnMOF** [d]	24	0.20	4	60	73.7
23	**ZnMOF** [b]	24	0.20	4	60	89.6
24	**ZnMOF** [e]	24	0.20	4	60	9.0

[a] Determined by ^{1}H NMR analysis (see Experimental part). Co-catalyst: [b] TBABr (0.4 mol%); [c] TBACl (0.4 mol%); [d] TBAI (0.4 mol%); [e] without TBABr.

To assess the essential role of the catalyst, we conducted a blank test, revealing only ca. 15% conversion of epoxide at 60 °C after 24 h (entry 8, Table 1). Additionally, we tested the activity of the simple metal salt $Zn(NO_3)_2{\cdot}6H_2O$ and ligand **H_3L** under the same conditions. $Zn(NO_3)_2{\cdot}6H_2O$ produced a conversion of ca. 51%, while **H_3L** converted notably lower at ca. 16% (entries 19 and 20, Table 1). Hence, the use of **ZnMOF** as the catalyst resulted in a substantially higher conversion of ca. 90%. This highlights the superior effectiveness of the **ZnMOF** catalyst over $Zn(NO_3)_2{\cdot}6H_2O$ in promoting this cycloaddition reaction.

The choice of co-catalyst can influence reaction steps, such as the nucleophilic attack and ring-opening of the epoxide (see below). We explored the influence of different co-catalysts, specifically TBABr, TBACl, and TBAI, under identical reaction conditions (entries 21–23, Table 1). Our results revealed a striking disparity in conversions based on the co-catalyst selection. TBABr stood out, achieving the highest conversion of ca. 90% at 60 °C and 4 MPa for 24 h. In contrast, parallel experiments with TBACl and TBAI resulted in much lower conversions (Table 1, entries 21 and 22), underscoring the superior performance of TBABr as a co-catalyst. When the catalytic reaction was performed without the co-catalyst (TBABr), the conversion dropped dramatically to approximately 9% (entry 24, Table 1),

demonstrating the crucial role of the co-catalyst in the reaction mechanism. The differences in conversion among co-catalysts can be attributed to various factors, including differences in reactivity and selectivity.

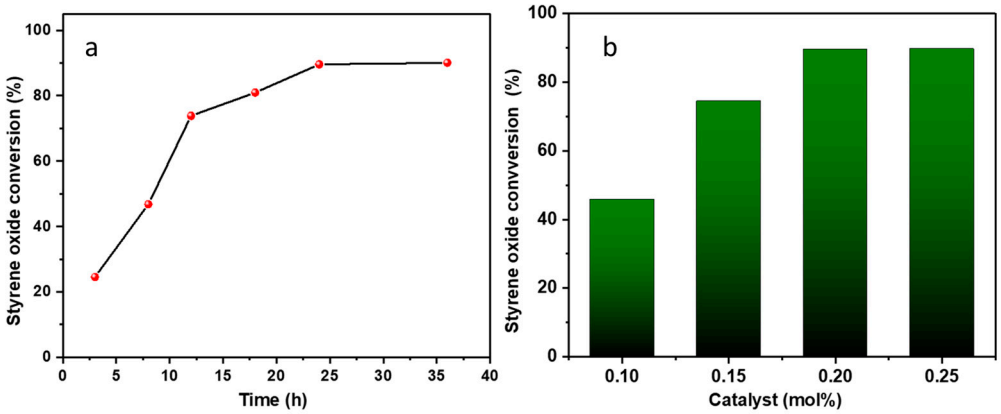

Figure 3. Influence of reaction time (**a**) and catalyst mol% (**b**) on conversion into styrene carbonate. Reaction conditions: (**a**) 4 MPa, 60 °C, 0.20 mol% of catalyst (**ZnMOF**) and 0.4% mol of co-catalyst (TBABr); (**b**) 4 MPa, 60 °C, 24 h, 0.10–0.25 mol% of catalyst (**ZnMOF**) and 0.4% mol of co-catalyst (TBABr).

Subsequently, under optimised conditions, we investigated the scope of the reaction with various substituted epoxides. The reaction conversions from five different epoxides ranged from ca. 17% to 100%. Propylene oxide, 1,2-butylene oxide, epichlorohydrin and *tert*-butyl glycidyl ether were converted to cyclic carbonates with high efficiency (entries 1–4, Table 2), while cyclohexene oxide resulted in a much lower conversion of ca. 17% (entry 5, Table 2), possibly on account of steric hindrance. No clear conversion dependence on the electronic properties of the epoxides is observed.

Table 2. Cycloaddition reaction of various epoxides and CO_2 catalysed by **ZnMOF** [a].

Entry	Substrate	Epoxide Conversion (%) [b]
1	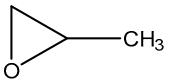	99.4
2	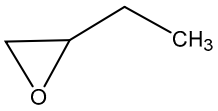	98.2
3	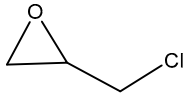	89.9
4	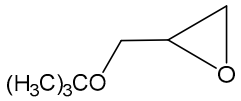	80.8
5	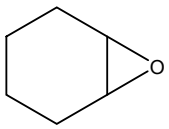	16.9

[a] Reaction conditions: epoxide (8.74 mmol), 0.20 mol% of catalyst (**ZnMOF**), 0.4 mol% cocatalyst (TBABr), 24 h, 4 MPa, 60 °C. [b] Determined by ^{1}H NMR analysis (Figures S8–S12).

We also evaluated the catalyst stability and reusability. Preliminary recycling experiments were performed using styrene oxide under optimised conditions which provided an indication of the catalyst's stability and recyclability. As can be observed in Figure 4, **ZnMOF** retained its catalytic activity without any noticeable decline across three consecutive runs. Its structural integrity was verified through IR analysis following the catalysis process (Figure S4).

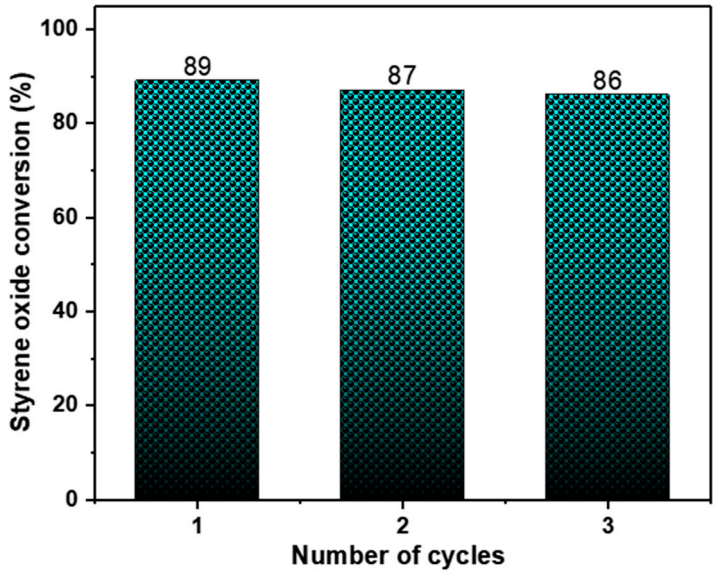

Figure 4. Recyclability of catalyst **ZnMOF**. Reaction conditions: epoxide (8.74 mmol), 0.20 mol% of catalyst (**ZnMOF**), 0.4 mol% cocatalyst (TBABr), 24 h, 4 MPa, 60 °C.

A plausible reaction mechanism of the CO_2 cycloaddition reaction with epoxides, based on literature proposals [41–44], is delineated in Figure 5 for the cycloaddition reaction catalysed by the **ZnMOF**. It begins with the chemical activation of epoxides through their interaction with Lewis acidic Zn sites (step 1, Figure 5). Subsequently, the activated epoxide undergoes nucleophilic attack by the co-catalyst TBABr, generating an alkoxide intermediate (step 2, Figure 5). This intermediate then combines with CO_2 to produce the cyclic carbonate product (steps 3 and 4, Figure 5). The last step regenerates the Zn active site, making it available for further catalytic cycles. The cyclic carbonate can be easily separated from the catalyst, and the **ZnMOF** can be reused for subsequent catalytic cycles. The high catalytic performance of **ZnMOF** is attributed to the synergistic effect of the MOF and TBABr.

Furthermore, the presence of tetrazole and amide functional groups in the ligand framework of the MOF can facilitate CO_2 cycloaddition reactions with epoxides through multiple mechanisms [43]. The Lewis basic site in the tetrazole moiety of the MOF can interact with CO_2 forming a Lewis acid–base adduct with activated CO_2 by weakening its carbon–oxygen bonds. This activation step lowers the energy barrier for subsequent reactions involving CO_2, ultimately enhancing the catalytic efficiency of the MOF. On the other hand, the hydrogen bonding capability of amide groups can stabilise reaction intermediates. Both groups can enhance the adsorption of reactants onto the MOF surface, promoting efficient reactant–catalyst interactions. These combined effects make MOFs containing these functional groups promising candidates for catalysing CO_2 cycloaddition reactions with epoxides [45].

In a comparative analysis of catalyst performance for the CO_2 cycloaddition with epoxides, we evaluated the effectiveness of our catalyst alongside several examples reported in the literature. Relevant parameters to consider are reaction temperature and pressure, reaction time, the type of substrate, the amount of catalyst, and also the type and the amount of co-catalyst that plays a crucial role. Although conducting direct comparisons is

quite complex due to differences in operating conditions, we have selected for comparison only reported Zn-based heterogeneous catalysts using styrene oxide as substrate and TBABr as co-catalyst. Caparisons are made in terms of TOF to normalise the catalytic activity with respect to the number of active Zn sites and reaction time as presented in Table 3.

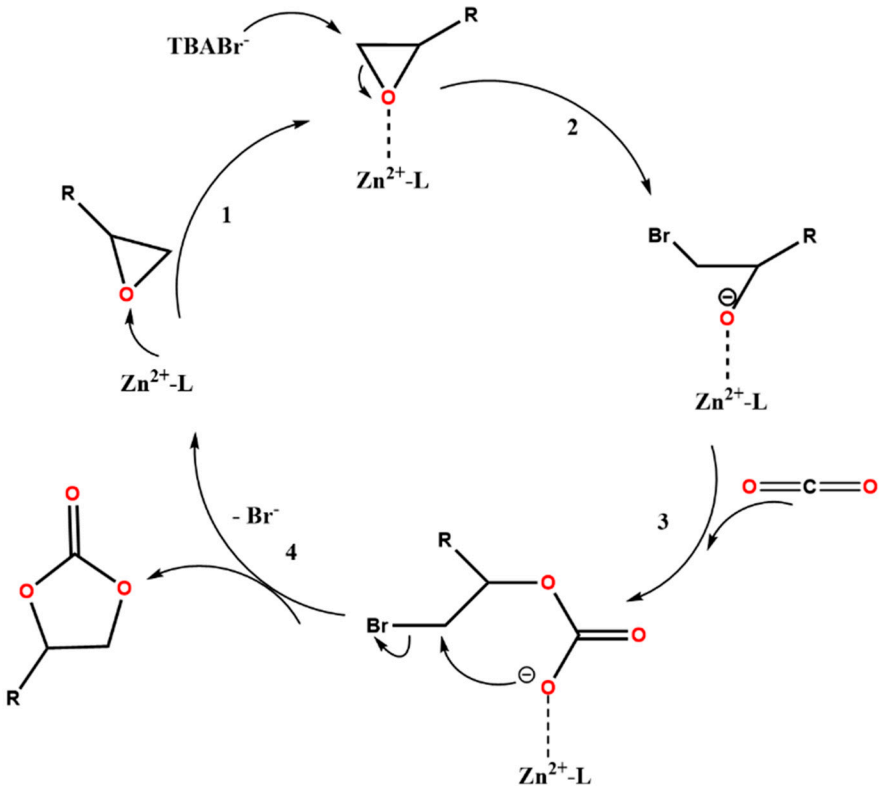

Figure 5. Proposed reaction pathway for the catalytic CO_2 cycloaddition with epoxides in the presence of **ZnMOF** and TBABr co-catalyst.

Table 3. Comparison of our **ZnMOF** catalyst with other Zn-based heterogeneous catalysts.

Catalyst	Zn (mol%)	TBABr (mol%)	T (°C)	p (MPa)	Time (h)	TOF (h^{-1})	Reference
ZnMOF	0.4	0.4	60	4.0	3	21	This work
Zn_4@POSS-1	1.0	4.0	100	0.1	4	10	[46]
Zn(salen)	2.0	-	50	5.0	24	1	[47]
MOF-205(M)	2.4	0.6	Rt	1.2	24	2	[41]
ZnMOF-1-NH_2	1.0	2.5	60	0.8	6	13	[43]
Zn(Bmic)(AT)	0.5	1.5	90	0.5	6	26	[48]
MOF-5-MIX	0.5	0.5	50	1.2	6	18	[49]
Zn(Py)(Atz)	0.6	0.9	60	1.5	24	5	[50]
Zn-2PDC	0.5	3.5	55	1.0	4	29	[51]
NIIC-10-Pr	2.0	1.5	80	0.2	20	2	[52]
Zn(dibpca)(OAc)	0.1	2.5	80	0.1	10	70	[53]

POSS = octa(3-aminopropyl)silsesquioxane; salen = salicylaldehydeethylenediamine; MOF-205(M) = [Zn_4O(2,6-NDC)$(BTB)_{4/3}$], 2,6-NDC: 2,6-naphthalenedicarboxylate, BTB: 1,3,5-tris(4-carboxyphenyl)benzene; MOF-5-MIX = $Zn(NO_3)\cdot 6H_2O$, 2-amino-terephthalic acid, 2-hydroxy-terephthalic acid; NIIC-10-Pr = $Zn(NO_3)\cdot 6H_2O$, thiophene-2,5-dicarboxylic acid, 1,4-diazo[2.2.2.]bicyclooctane; Bmic = 1-benzimidazole-5-carboxylate; AT = 5-aminotetrazole; Py = 3,5-pyridinedicarboxylate; Atz = 3-amino-1,2,4-triazole; PDC = 1,1′-(propane-1,3-diyl)bis(1*H*-pyrazole-3,5-dicarboxylate); dibpca = 3′,5′-di(1H-imidazol-1-yl)-[1,1′-biphenyl]-4-carboxylate: OAc = acetate.

The results presented in Table 3 indicate that taking into account the differences in operating conditions, our catalyst exhibits a competitive catalytic activity compared to other reported heterogeneous zinc catalysts. Among those presented in the Table, although most of them have tested slightly lower pressures, only catalysts that used higher

amounts of co-catalyst showed superior activities. Nevertheless, it should be noted that the amount of co-catalyst has a very significant effect since it participates in the reaction rate-determining step.

3. Synthesis and Characterisation

*3.1. Synthesis of 4-((4-(1H-Tetrazol-5-yl)Phenyl)Carbamoyl)Benzoic Acid (**H_3L**)*

In the initial step, a solution containing methyl 4-(chlorocarbonyl)benzoate (0.396 g, 2 mmol) in 20 mL of anhydrous THF was carefully added dropwise to a solution containing 4-aminobenzonitrile (0.236 g, 2 mmol) and triethylamine (600 µL, 2 mmol) in 80 mL of anhydrous THF. The resulting mixture was stirred for 24 h. The resulting white product, methyl 4-((4-cyanophenyl)carbamoyl)benzoate, was isolated through filtration, subjected to THF washing, and subsequently dried under vacuum. This product was utilised in the subsequent step without any further purification.

In the subsequent step, methyl 4-((4-cyanophenyl)carbamoyl)benzoate (0.250 g, 0.90 mmol) was dissolved in 50 mL of anhydrous DMF. To this solution, NaN_3 (0.116 g, 1.8 mmol) and NH_4Cl (0.094 g, 1.8 mmol) were added, and the mixture was refluxed at 120 °C for 24 h, following a previously documented procedure [28,29,36]. Subsequently, the reaction mixture was poured into ice-cooled water and acidified with dilute hydrochloric acid (HCl). This resulted in the formation of an off-white precipitate, which was separated by filtration, washed with water, and collected.

The product obtained in the previous step was then subjected to hydrolysis using NaOH in a mixture of methanol and water (4:1, *v*/*v*), following a previously established protocol [28,32,33]. The desired product, **H_3L**, was isolated by filtration and washed with water until it reached a neutral pH. Yield: 0.1 g, 40%. Anal. Calcd for $C_{15}H_{11}N_5O_3$: C, 58.25; H, 3.59; N, 22.64. Found: C, 58.72; H, 4.13; N, 23.03. FT-IR (KBr, cm^{-1}): 3383 (bs), 2547 (mb), 1691 (s), 1590 (s), 1507 (s), 1378 (s), 1320 (m), 1196 (m), 1109 (w), 1057 (w), 961 (s), 759 (s), 883 (s), 730 (s), 528 (w); ^{1}H-NMR (300 MHz, DMSO-d_6, δ ppm): 13.41 (s, 1H, –COOH), 10.82 (s, 1H, NH), 8.09–7.83 (m, 8H, HAr). ^{13}C-NMR (77 MHz, DMSO-d_6, δ ppm): 167.1, 165.9, 143.7, 138.8, 134.2, 133.5, 129.8, 128.4, 120.7, 119.5, 105.9.

*3.2. Synthesis of $[Zn_2(\mu_3\text{-}1\kappa N,2\kappa N',3\kappa O\text{-}HL)_2(DMF)_2]_n \cdot nH_2O$ (**ZnMOF**)*

An aqueous solution of $Zn(NO_3)_2 \cdot 6H_2O$ (13 mg, 0.022 mmol) was added to previously dissolved 10 mg of **H_3L** (0.022 mmol) in a 1 mL of DMF of an 8 mL glass vessel and tightly sealed. The solution was then subjected to heating at 80 °C for 36 h. Following this reaction period, the solution was gradually cooled to room temperature, leading to the formation of white crystals identified as the **ZnMOF**. Yield: 0.006 g, 46%. Anal. Calcd for $C_{36}H_{34}N_{12}O_9Zn_2$: C, 47.54; H, 3.77; N, 18.48. Found: C, 47.70; H, 3.80; N, 18.52. IR (KBr/pellet, cm^{-1}): 3080 (w, br), 1666 (w), 1596 (s), 1516 (w), 1428 (s), 1388 (s), 1331 (w), 1296 (m, sh), 1210 (m), 1095 (w), 1024 (m), 897 (m), 841 (m), 732 (s, br), 573 (m), 538 (m).

4. Conclusions

This study elucidated the synthesis, characterisation and catalytic potential of a novel nitrogen-rich Zn(II) MOF. The structural analysis revealed a 2D framework with small rectangular channels and the topological analysis demonstrated a 3-connected uninodal net with a Shubnikov plane net, highlighting the framework's unique structural features.

The **ZnMOF** catalytic activity in CO_2 cycloaddition reactions with styrene oxide proved notable, achieving a noteworthy 90%. Furthermore, the conversion of five different epoxides showed a wide conversion range, spanning from 17% to 100%. Propylene oxide, 1,2-butylene oxide, epichlorohydrin, and *tert*-butyl glycidyl ether displayed remarkable reactivity for cyclic carbonate production. In contrast, cyclohexene oxide presented a much lower conversion in accord with a higher steric hindrance. Importantly, the catalyst also demonstrated excellent stability and reusability over three consecutive runs.

The **ZnMOF** porosity characteristics, including a mesoporous structure with a predominant pore size distribution within the 10–24 nm range and a substantial BET surface

area of 30.6 m^2/g, could have significantly enhanced the catalytic performance of **ZnMOF** by facilitating efficient reactant adsorption and mass transport. In addition, the presence of nitrogen-rich tetrazole and amide functional groups in the MOF ligand framework may have also promoted the CO_2 cycloaddition reaction with an epoxide through mechanisms concerning its Lewis basic and hydrogen bonding sites.

In summary, this study not only presents the synthesis and characterisation of a novel nitrogen-rich Zn(II) MOF but also showcases its promising catalytic potential in the CO_2 cycloaddition reaction with epoxides. The optimisation of reaction conditions and excellent stability make this **ZnMOF** a noteworthy candidate for further exploration in green and sustainable catalysis applications.

Supplementary Materials: The following supporting information can be downloaded at: https://www.mdpi.com/article/10.3390/catal14010006/s1, Figures S1–S12 contain ATR-IR, 1H, 13C-NMR, PXRD and TGA. Tables S1–S3 contain the crystallographic data of **ZnMOF** [54–57].

Author Contributions: A.P.: conceptualisation; formal analysis; investigation; methodology; writing—original draft, review, and editing. I.M.G.: catalysis; investigation; methodology; formal analysis; data curation. A.K.: single crystal X-ray crystallography; writing—original draft. R.A.K.: formal analysis; writing—original draft. M.F.C.G.d.S.: formal analysis; writing—review and editing. A.V.M.N.: Supervision; writing—review and editing. A.J.L.P.: writing—review and editing. All authors have read and agreed to the published version of the manuscript.

Funding: This research was funded by the FCT and IST, Portugal, for financial support through "DL/57/2017" (contract no. IST-ID/197/2019). I.M.G. is grateful to the State Program for Increasing the International Competitiveness of the higher education system of the Republic of Azerbaijan in 2019–2023, Ministry of Science and Education Republic of Azerbaijan. R.A.K. gratefully acknowledged Researchers Supporting Project (Project number, RSP2023R400), King Saud University, Riyadh, KSA. This work has also been partially supported by the Fundação para a Ciência e a Tecnologia (FCT), Portugal, through projects UIDB/00100/2020, UIDP/00100/2020, and LA/P/0056/2020 of Centro de Química Estrutural. M.F.C.G.d.S. acknowledges financial support by Fundação para a Ciência e Tecnologia FCT/MCTES through project 2022.02069.PTDC. A.V.M.N. acknowledges financial support by Fundação para a Ciência e Tecnologia FCT/MCTES through project MIT-EXPL/CS/0052/2021 and to the Associate Laboratory for Green Chemistry—LAQV which is financed by National Funds from FCT/MCTES (UIDB/50006/2020 and UIDP/50006/2020). The authors also acknowledge the Portuguese NMR Network (IST-UL Centre) for access to the NMR facility.

Data Availability Statement: Data are contained within the article and Supplementary Materials.

Conflicts of Interest: The authors declare no conflict of interest.

References

1. Coluccia, M.; Parisse, V.; Guglielmi, P.; Giannini, G.; Secci, D. Metal-Organic Frameworks (MOFs) as Biomolecules Drug Delivery Systems for Anticancer Purposes. *Eur. J. Med. Chem.* **2022**, *244*, 114801. [CrossRef] [PubMed]
2. Dong, A.; Chen, D.; Li, Q.; Qian, J. Metal-Organic Frameworks for Greenhouse Gas Applications. *Small* **2023**, *19*, 2201550. [CrossRef] [PubMed]
3. Wang, J.X.; Yin, J.; Shekhah, O.; Bakr, O.M.; Eddaoudi, M.; Mohammed, O.F. Energy Transfer in Metal-Organic Frameworks for Fluorescence Sensing. *ACS Appl. Mater. Interfaces* **2022**, *14*, 9970–9986. [CrossRef] [PubMed]
4. Li, Y.M.; Hu, J.; Zhu, M. Confining Atomically Precise Nanoclusters in Metal–Organic Frameworks for Advanced Catalysis. *Coord. Chem. Rev.* **2023**, *495*, 215364. [CrossRef]
5. Li, P.Z.; Wang, X.J.; Zhang, K.; Nalaparaju, A.; Zou, R.; Zou, R.; Jiang, J.; Zhao, Y. 'Click'-Extended Nitrogen-Rich Metal–Organic Frameworks and Their High Performance in CO_2-Selective Capture. *Chem. Commun.* **2014**, *50*, 4683–4685. [CrossRef] [PubMed]
6. Cheng, W.C.; Chen, J.M.; Deng, L.; Huang, H.S.; Zhang, J.G.; Zhang, T.L.; Li, Z.M. High-Efficiency Catalysis of Nitrogen-Rich Metal-Organic Frameworks and Their Derivatives for the Thermal Decomposition of Ammonium Perchlorate. *Energ. Mater. Front.* **2023**, *4*, 37–43. [CrossRef]
7. Cao, S.M.; Chen, H.B.; Dong, B.X.; Zheng, Q.H.; Ding, Y.X.; Liu, M.J.; Qian, S.L.; Teng, Y.L.; Li, Z.W.; Liu, W.L. Nitrogen-Rich Metal-Organic Framework Mediated Cu–N–C Composite Catalysts for the Electrochemical Reduction of CO_2. *J. Energy Chem.* **2021**, *54*, 555–563. [CrossRef]
8. Guo, C.R.; Ying, Y.M.; Yu, M.; Xiong, Y.; Liu, X.G.; Zhao, Z. Nitrogen-Rich Tetraphenylethene-Based Luminescent Metal-Organic Framework for Efficient Detection of Carcinogens. *ACS Omega* **2021**, *6*, 2177–2183. [CrossRef]

9. Mohan, M.; Essalhi, M.; Durette, D.; Rana, L.K.; Ayevide, F.K.; Maris, T.; Duong, A. A Rational Design of Microporous Nitrogen-Rich Lanthanide Metal-Organic Frameworks for CO_2/CH_4 Separation. *ACS Appl. Mater. Interfaces* **2020**, *12*, 50619–50627. [CrossRef]
10. Pachfule, P.; Banerjee, R. Porous Nitrogen Rich Cadmium-Tetrazolate Based Metal Organic Framework (MOF) for H_2 and CO_2 Uptake. *Cryst. Growth Des.* **2011**, *11*, 5176–5181. [CrossRef]
11. Wu, Y.L.; Yang, G.P.; Cheng, S.; Qian, J.; Fan, D.; Wang, Y.Y. Facile Incorporation of Au Nanoparticles into an Unusual Twofold Entangled Zn(II)-MOF with Nanocages for Highly Efficient CO_2 Fixation under Mild Conditions. *ACS Appl. Mater. Interfaces* **2019**, *11*, 47437–47445. [CrossRef] [PubMed]
12. Han, C.; Zhang, X.; Huang, S.; Hu, Y.; Yang, Z.; Li, T.T.; Li, Q.; Qian, J. MOF-on-MOF-Derived Hollow Co_3O_4/In_2O_3 Nanostructure for Efficient Photocatalytic CO_2 Reduction. *Adv. Sci.* **2023**, *10*, 2300797. [CrossRef] [PubMed]
13. Xu, L.; Qiao, J.; Xu, S.; Zhao, X.; Gong, W.; Huang, T. Constructing Strategies and Applications of Nitrogen-Rich Energetic Metal–Organic Framework Materials. *Catalysts* **2020**, *10*, 690. [CrossRef]
14. Zhang, W.; Xu, C.H.; Zheng, H.; Li, R.; Zhou, K. Oxygen-Rich Cobalt–Nitrogen–Carbon Porous Nanosheets for Bifunctional Oxygen Electrocatalysis. *Adv. Funct. Mater.* **2022**, *32*, 2200763. [CrossRef]
15. Chen, C.; Jia, M.; Wang, G.; Li, X.; Li, S. High and Selective CO_2 Uptake in a Nitrogen-Rich Pillar-Layered Metal Organic Framework. *RSC Adv.* **2015**, *5*, 104932–104935. [CrossRef]
16. Ji, L.Q.; Yang, J.; Zhang, Z.Y.; Qian, Y.; Su, Z.; Han, M.; Liu, H.K. Enhanced Catalytic Performance for Oxygen Reduction Reaction Derived from Nitrogen-Rich Tetrazolate-Based Heterometallic Metal-Organic Frameworks. *Cryst. Growth Des.* **2019**, *19*, 2991–2999. [CrossRef]
17. Mao, Y.; Wang, Q.; Yu, L.; Qian, H.; Deng, S.; Xiao, W.; Zhao, D.; Chen, C. A 2-Fold Interpenetrated Nitrogen-Rich Metal-Organic Framework for Rapid and Selective Adsorption of Congo Red. *Inorg. Chem.* **2020**, *59*, 8213–8219. [CrossRef]
18. Gao, C.L.; Nie, J.Y. Preferential CO_2 Adsorption and Theoretical Simulation of a Cu(II)-Based Metal-Organic Framework with Open-Metal Sites and Basic Groups. *Inorg. Chem. Commun.* **2019**, *102*, 199–202. [CrossRef]
19. Peng, L.L.; Zhou, W.F.; Xu, W.F.; Liu, Y.; Zhou, C.S.; Xie, J.; Tang, K.W. Nitrogen-Rich Covalent Phosphazene-Based Framework for Efficient Removal of Lead(Ii) Ions. *New J. Chem.* **2023**, *47*, 6095–6101. [CrossRef]
20. Xu, J.G.; Yan, Y.F.; Li, X.Z.; Zheng, F.K.; Guo, G.C. A New Sensitive Structural Motif Inlaying the Azides and Tetrazole-Based Rigid 3D Energetic MOFs: Highly Sensitive Primary Explosives with Excellent Thermal Stability. *J. Chem. Eng.* **2022**, *429*, 132451. [CrossRef]
21. Zhang, R.; Meng, D.X.; Ge, F.Y.; Huang, J.H.; Wang, L.F.; Xv, Y.K.; Liu, X.G.; Meng, M.M.; Yan, H.; Lu, Z.Z.; et al. Tetrazole-Based Porous Metal-Organic Frameworks for Selective CO_2 Adsorption and Isomerization Studies. *Dalton Trans.* **2020**, *49*, 2145–2150. [CrossRef] [PubMed]
22. Shi, D.; Guo, X.; Lai, T.; Zheng, K.; Wu, Q.; Sun, C.; He, C.; Zhao, J. A Tetrazole-Containing Triphenylamine-Based Metal–Organic Framework: Synthesis and Photocatalytic Oxidative C–C Coupling Reaction. *Inorg. Chem. Commun.* **2019**, *105*, 9–12. [CrossRef]
23. Li, Q.; Yu, M.H.; Xu, J.; Li, A.L.; Hu, T.L.; Bu, X.H. Two New Metal-Organic Frameworks Based on Tetrazole-Heterocyclic Ligands Accompanied by in Situ Ligand Formation. *Dalton Trans.* **2017**, *46*, 3223–3228. [CrossRef] [PubMed]
24. Song, W.C.; Li, J.R.; Song, P.C.; Tao, Y.; Yu, Q.; Tong, X.L.; Bu, X.H. Tuning the Framework Topologies of CoII-Doped Zn II-Tetrazole-Benzoate Coordination Polymers by Ligand Modifications: Structures and Spectral Studies. *Inorg. Chem.* **2009**, *48*, 3792–3799. [CrossRef] [PubMed]
25. Sun, J.Y.; Wang, L.; Zhang, D.J.; Li, D.; Cao, Y.; Zhang, L.Y.; Zeng, S.L.; Pang, G.S.; Fan, Y.; Xu, J.N.; et al. Construction of Metal-Organic Coordination Polymers Derived from 4-Substituted Tetrazole-Benzoate Ligands: Synthesis, Structure, Luminescence, and Magnetic Behaviors. *CrystEngComm* **2013**, *15*, 3402–3411. [CrossRef]
26. Ordonez, C.; Kinnibrugh, T.L.; Xu, H.; Lindline, J.; Timofeeva, T.; Wei, Q. Synthesis of Framework Isomer MOFs Containing Zinc and 4-Tetrazolyl Benzenecarboxylic Acid via a Structure Directing Solvothermal Approach. *Crystals* **2015**, *5*, 193–205. [CrossRef]
27. Li, Y.; Xu, G.; Zou, W.Q.; Wang, M.S.; Zheng, F.K.; Wu, M.F.; Zeng, H.Y.; Guo, G.C.; Huang, J.S. A Novel Metal-Organic Network with High Thermal Stability: Nonlinear Optical and Photoluminescent Properties. *Inorg. Chem.* **2008**, *47*, 7945–7947. [CrossRef]
28. Paul, A.; Karmakar, A.; Guedes da Silva, M.F.C.; Pombeiro, A.J.L. Amide Functionalized Metal-Organic Frameworks for Diastereoselective Nitroaldol (Henry) Reaction in Aqueous Medium. *RSC Adv.* **2015**, *5*, 87400–87410. [CrossRef]
29. Paul, A.; Das, K.; Karmakar, A.; Guedes Da Silva, M.F.C.; Pombeiro, A.J.L. A Mechanistic Insight into the Rapid and Selective Removal of Congo Red by an Amide Functionalised Zn(II) Coordination Polymer. *Dalton Trans.* **2020**, *49*, 12970–12984. [CrossRef]
30. Karmakar, A.; Paul, A.; Rúbio, G.M.D.M.; Soliman, M.M.A.; Guedes da Silva, M.F.C.; Pombeiro, A.J.L. Highly Efficient Bifunctional Amide Functionalized Zn and Cd Metal Organic Frameworks for One-Pot Cascade Deacetalization–Knoevenagel Reactions. *Front. Chem.* **2019**, *7*, 699. [CrossRef]
31. Paul, A.; Martins, L.M.D.R.S.; Karmakar, A.; Kuznetsov, M.L.; C Guedes da Silva, M.F.; Pombeiro, A.J.L. Zn(II)-to-Cu(II) Transmetalation in an Amide Functionalized Complex and Catalytic Applications in Styrene Oxidation and Nitroaldol Coupling. *Molecules* **2020**, *25*, 2644. [CrossRef] [PubMed]
32. Paul, A.; Martins, L.M.D.R.S.; Karmakar, A.; Kuznetsov, M.L.; Novikov, A.S.; Guedes da Silva, M.F.C.; Pombeiro, A.J.L. Environmentally Benign Benzyl Alcohol Oxidation and C–C Coupling Catalysed by Amide Functionalized 3D Co(II) and Zn(II) Metal Organic Frameworks. *J. Catal.* **2020**, *385*, 324–337. [CrossRef]

33. Paul, A.; Upadhyay, K.K.; Backović, G.; Karmakar, A.; Vieira Ferreira, L.F.; Šljukić, B.; Montemor, M.F.; Guedes Da Silva, M.F.C.; Pombeiro, A.J.L. Versatility of Amide-Functionalized Co(II) and Ni(II) Coordination Polymers: From Thermochromic-Triggered Structural Transformations to Supercapacitors and Electrocatalysts for Water Splitting. *Inorg. Chem.* **2020**, *59*, 16301–16318. [CrossRef] [PubMed]
34. Fan, S.C.; Li, Y.T.; Wang, Y.; Wang, J.W.; Xue, Y.Y.; Li, H.P.; Li, S.N.; Zhai, Q.G. Amide-Functionalized Metal-Organic Frameworks Coupled with Open Fe/Sc Sites for Efficient Acetylene Purification. *Inorg. Chem.* **2021**, *60*, 18473–18482. [CrossRef] [PubMed]
35. Lin, Y.; Kong, C.; Chen, L. Amine-Functionalized Metal-Organic Frameworks: Structure, Synthesis and Applications. *RSC Adv.* **2016**, *6*, 32598–32614. [CrossRef]
36. Moi, R.; Nath, K.; Ghosh, D.; Biradha, K. Metal-Organic Gels of Tris-Tetrazole-tri-Amido Molecule with Co(II) and Ni(II) as Electrocatalysts for OER: Effect of Metal Ion, Porosity and Morphology on the Catalysis of MOGs. *ChemCatChem* **2023**, *15*, e202300694. [CrossRef]
37. Zhou, L.; Xue, Y.S.; Xu, Y.; Zhang, J.; Du, H. Bin Two Photoluminescent Metal-Organic Frameworks Based on a BODIPY-Derived Bipyridine Ligand. *CrystEngComm* **2013**, *15*, 7315–7320. [CrossRef]
38. Peedikakkal, A.M.P.; Aljund, I.H. Upgrading the Hydrogen Storage of Mof-5 by Post-Synthetic Exchange with Divalent Metal Ions. *Appl. Sci.* **2021**, *11*, 11687. [CrossRef]
39. Yang, L.; Powell, D.R.; Houser, R.P. Structural Variation in Copper(I) Complexes with Pyridylmethylamide Ligands: Structural Analysis with a New Four-Coordinate Geometry Index, T4. *Dalton Trans.* **2007**, *9*, 955–964. [CrossRef]
40. Ambroz, F.; Macdonald, T.J.; Martis, V.; Parkin, I.P. Evaluation of the BET Theory for the Characterization of Meso and Microporous MOFs. *Small Methods* **2018**, *2*, 1800173. [CrossRef]
41. Babu, R.; Roshan, R.; Kathalikkattil, A.C.; Kim, D.W.; Park, D.W. Rapid, Microwave-Assisted Synthesis of Cubic, Three-Dimensional, Highly Porous MOF-205 for Room Temperature CO_2 Fixation via Cyclic Carbonate Synthesis. *ACS Appl. Mater. Interfaces* **2016**, *8*, 33723–33731. [CrossRef] [PubMed]
42. Kathalikkattil, A.C.; Roshan, R.; Tharun, J.; Babu, R.; Jeong, G.S.; Kim, D.W.; Cho, S.J.; Park, D.W. A Sustainable Protocol for the Facile Synthesis of Zinc-Glutamate MOF: An Efficient Catalyst for Room Temperature CO_2 Fixation Reactions under Wet Conditions. *Chem. Commun.* **2016**, *52*, 280–283. [CrossRef] [PubMed]
43. Patel, P.; Parmar, B.; Kureshy, R.I.; Khan, N.U.H.; Suresh, E. Amine-Functionalized Zn(II) MOF as an Efficient Multifunctional Catalyst for CO_2 Utilization and Sulfoxidation Reaction. *Dalton Trans.* **2018**, *47*, 8041–8051. [CrossRef] [PubMed]
44. Guo, L.; Lamb, K.J.; North, M. Recent Developments in Organocatalysed Transformations of Epoxides and Carbon Dioxide into Cyclic Carbonates. *Green. Chem.* **2021**, *23*, 77–118. [CrossRef]
45. Maia, R.A.; Louis, B.; Gao, W.; Wang, Q. CO_2 adsorption Mechanisms on MOFs: A Case Study of Open Metal Sites, Ultra-Microporosity and Flexible Framework. *React. Chem. Eng.* **2021**, *6*, 1118–1133. [CrossRef]
46. Janeta, M.; Lis, T.; Szafert, S. Zinc Imine Polyhedral Oligomeric Silsesquioxane as a Quattro-Site Catalyst for the Synthesis of Cyclic Carbonates from Epoxides and Low-Pressure CO_2. *Chem.—Eur. J.* **2020**, *26*, 13686–13697. [CrossRef] [PubMed]
47. Kuznetsova, S.A.; Rulev, Y.A.; Larionov, V.A.; Smol'yakov, A.F.; Zubavichus, Y.V.; Maleev, V.I.; Li, H.; North, M.; Saghyan, A.S.; Belokon, Y.N. Self-Assembled Ionic Composites of Negatively Charged Zn(Salen) Complexes and Triphenylmethane Derived Polycations as Recyclable Catalysts for the Addition of Carbon Dioxide to Epoxides. *ChemCatChem* **2019**, *11*, 511–519. [CrossRef]
48. Li, Y.; Zhang, X.; Lan, J.; Xu, P.; Sun, J. Porous Zn(Bmic)(AT) MOF with Abundant Amino Groups and Open Metal Sites for Efficient Capture and Transformation of CO_2. *Inorg. Chem.* **2019**, *58*, 13917–13926. [CrossRef]
49. Kurisingal, J.F.; Rachuri, Y.; Gu, Y.; Choe, Y.; Park, D.W. Multi-Variate Metal Organic Framework as Efficient Catalyst for the Cycloaddition of CO_2 and Epoxides in a Gas-Liquid-Solid Reactor. *J. Chem. Eng.* **2020**, *386*, 121700. [CrossRef]
50. Lan, J.; Qu, Y.; Zhang, X.; Ma, H.; Xu, P.; Sun, J. A Novel Water-Stable MOF Zn(Py)(Atz) as Heterogeneous Catalyst for Chemical Conversion of CO_2 with Various Epoxides under Mild Conditions. *J. CO2 Util.* **2020**, *35*, 216–224. [CrossRef]
51. Li, Y.; Zhang, X.; Lan, J.; Li, D.; Wang, Z.; Xu, P.; Sun, J. A High-Performance Zinc-Organic Framework with Accessible Open Metal Sites Catalyzes CO_2 and Styrene Oxide into Styrene Carbonate under Mild Conditions. *ACS Sustain. Chem. Eng.* **2021**, *9*, 2795–2803. [CrossRef]
52. Bondarenko, G.N.; Ganina, O.G.; Lysova, A.A.; Fedin, V.P.; Beletskaya, I.P. Cyclic Carbonates Synthesis from Epoxides and CO_2 over NIIC-10 Metal-Organic Frameworks. *J. CO2 Util.* **2021**, *53*, 101718. [CrossRef]
53. Li, H.J.; Zhang, X.Y.; Huang, K.; Qin, D. Bin A Novel 2D Zinc(II)-Organic Framework for Efficient Catalytic Cycloaddition of CO_2 with Epoxides. *Polyhedron* **2022**, *220*, 115850. [CrossRef]
54. Bruker. *APEX2*; Bruker AXS Inc.: Madison, WI, USA, 2012.
55. Sheldrick, G.M. *SADABS Program for Empirical Absorption Correction*; University of Gottingen: Göttingen, Germany, 2000. [CrossRef]
56. Sheldrick, G.M. Crystal Structure Refinement with SHELXL. *Acta Crystallogr. C Struct. Chem.* **2015**, *71*, 3–8. [CrossRef]
57. Farrugia, L.J. WinGX and ORTEP for Windows: An Update. *J. Appl. Crystallogr.* **2012**, *45*, 849–854. [CrossRef]